Organic haze on Titan and the early Earth

Melissa G. Trainer*, Alexander A. Pavlov†, H. Langley DeWitt‡, Jose L. Jimenez‡, Christopher P. McKay§, Owen B. Toon¶, and Margaret A. Tolbert‡‖

*Laboratory for Atmospheric and Space Physics, University of Colorado, UCB 392, Boulder, CO 80309; †Department of Planetary Sciences Lunar and Planetary Laboratory, University of Arizona, 1629 East University Boulevard, Tucson, AZ 85721; ‡Department of Chemistry and Biochemistry and Cooperative Institute for Research in Environmental Sciences, University of Colorado, UCB 216, Boulder, CO 80309; §Space Science Division, NASA Ames Research Center, Moffett Field, CA 94035; and ¶Laboratory for Atmospheric and Space Physics and Department of Atmospheric and Oceanic Sciences, University of Colorado, UCB 392, Boulder, CO 80309

This contribution is part of the special series of Inaugural Articles by members of the National Academy of Sciences elected on April 20, 2004.

Contributed by Margaret A. Tolbert, September 27, 2006

Recent exploration by the Cassini/Huygens mission has stimulated a great deal of interest in Saturn's moon, Titan. One of Titan's most captivating features is the thick organic haze layer surrounding the moon, believed to be formed from photochemistry high in the CH_4/N_2 atmosphere. It has been suggested that a similar haze layer may have formed on the early Earth. Here we report laboratory experiments that demonstrate the properties of haze likely to form through photochemistry on Titan and early Earth. We have used a deuterium lamp to initiate particle production in these simulated atmospheres from UV photolysis. Using a unique analysis technique, the aerosol mass spectrometer, we have studied the chemical composition, size, and shape of the particles produced as a function of initial trace gas composition. Our results show that the aerosols produced in the laboratory can serve as analogs for the observed haze in Titan's atmosphere. Experiments performed under possible conditions for early Earth suggest a significant optical depth of haze may have dominated the early Earth's atmosphere. Aerosol size measurements are presented, and implications for the haze layer properties are discussed. We estimate that aerosol production on the early Earth may have been on the order of 10^{14} g·year^{-1} and thus could have served as a primary source of organic material to the surface.

planetary atmospheres | tholins | atmospheric aerosol | Archaen | astrobiology

Titan has long been a subject of interest, because it provides an excellent example of abiotic processing of organic material. The irradiation of the CH_4/N_2 atmosphere with sunlight and energetic electrons leads to the formation of aerosol particles, which aggregate into fractal agglomerates and generate a thick haze layer. Until the recent Cassini/Huygens mission, this haze layer obscured the moon's surface (1). Specific mechanisms for particle formation are not known, but they have been a major focus of attempts to understand the chemistry in Titan's atmosphere. Observed gaseous constituents such as C_2H_2, C_2H_4, C_2H_6, C_4H_2, C_6H_6, and HCN provide evidence of the active pathways toward aerosol formation (2–4). Results from the Huygens Probe show the presence of HCN and NH_3 within the particles but have not yet provided information on the overall chemical structure (5). Characterization of the chemical makeup of laboratory analogs, formed mostly as films produced in discharges, indicate that the haze aerosols are likely comprised of high-molecular-weight organic species including aromatic and aliphatic structures with some evidence of C—N bonding such as amines, imines, and nitriles (6–11).

Yung *et al.* (12) estimated that although the N-chemistry observed in the aerosols derives from energetic electrons in Saturn's magnetosphere, the majority of the organic constituents observed in Titan's atmosphere can be accounted for by photolysis. Other work studying production pathways concluded that polycyclic aromatic hydrocarbons formed through photochemistry were the primary contributors to the aerosol mass (13). Despite these positive modeling results, there have been no laboratory studies to directly measure the properties of aerosols expected from UV irradiation of CH_4 in a simulated Titan atmosphere. Adamkovics and Boering (14) used the detection of gas-phase products of CH_4 irradiation to infer the number of C—C bonds present in particle form, but did not directly measure aerosol properties or formation rates. Tran *et al.* (15, 16) used a low-pressure Hg lamp with primary emissions at 185 and 254 nm to produce films from the photodissociation of trace species (C_2H_2, etc.) rather than the direct photolysis of CH_4. Here, we describe a study in which the properties of aerosols formed from direct irradiation of CH_4 with a continuum VUV source are measured and discussed with relevance to Titan. We will show that the properties of the photochemical aerosols appear similar to those measured for Titan's haze layer, and that the rate of aerosol production is proportional to the rate of CH_4 photolysis.

In addition to its attraction as a planetary subject, the organic chemistry on Titan has captured interest as a possible analog for the early Earth (17, 18). The atmospheric composition of the early Earth before the rise of O_2 is a subject of debate. An atmosphere of only N_2/CO_2 raises concerns because it would not produce biologically interesting organic molecules, and geologic evidence restricts levels of CO_2, indicating that it was not the sole greenhouse gas (19). Tian *et al.* (20) showed that the prebiotic atmosphere may have contained large concentrations of H_2 in combination with CO_2 and CH_4. After the appearance of life, the atmospheric level of CH_4 would have risen, owing to a large flux of CH_4 from methanogen populations and a long chemical lifetime of CH_4 in the anoxic environment (21, 22). An atmosphere with ≈1,000 ppmv each of CH_4 and CO_2 would counteract the faint young sun sufficiently to keep temperatures above freezing and is a plausible scenario for the early Earth after the origin of life (23). It has been suggested that if the early Earth atmosphere contained significant amounts of CH_4, then photochemistry like that on Titan could be an important source of organics. However, with CO_2 also present in the atmosphere, the haze photochemistry would likely be different from what is currently observed for Titan. Attempts at modeling the effects of an early Earth haze layer suffer because of a lack of laboratory data for haze formation in CH_4/CO_2 atmospheres (22, 24). Some workers have studied organics formed in environments including CO, N_2, and CH_4, but these have either been focused on Titan conditions (25) or have looked only at amino acid production for

Author contributions: M.G.T., A.A.P., C.P.M., O.B.T., and M.A.T. designed research; M.G.T. and H.L.D. performed research; J.L.J. contributed new reagents/analytic tools; M.G.T., A.A.P., J.L.J., C.P.M., O.B.T., and M.A.T. analyzed data; and M.G.T., A.A.P., O.B.T., and M.A.T. wrote the paper.

The authors declare no conflict of interest.

Abbreviations: AMS, aerosol mass spectrometer; SMPS, scanning mobility particle sizer.

‖To whom correspondence should be addressed. E-mail: tolbert@cires.colorado.edu.

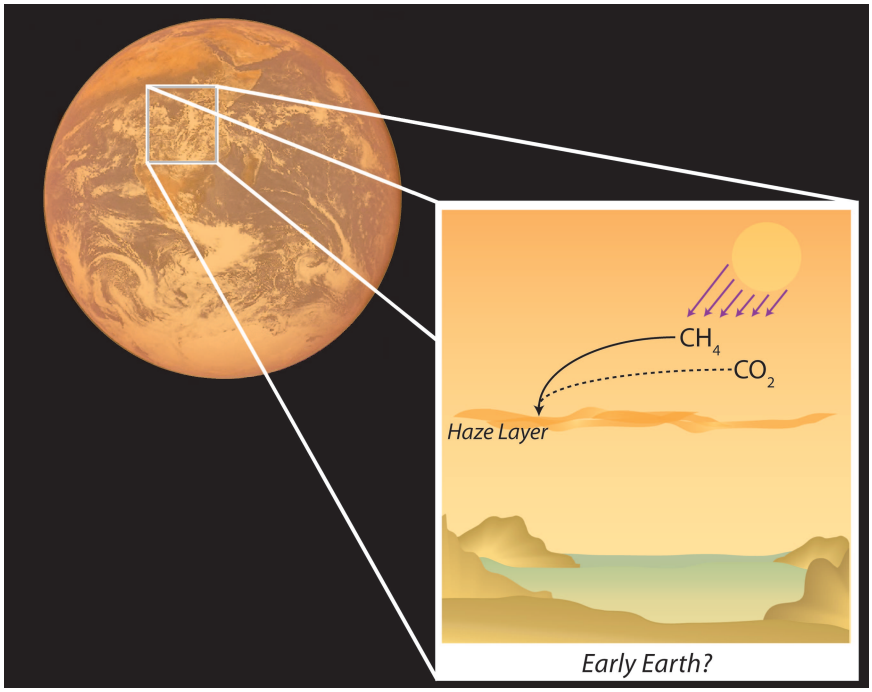

Fig. 1. A hazy early Earth? It has been proposed that if the early Earth's atmosphere contained CH_4, photochemical formation of an organic haze layer may have made the Earth's appearance very similar to that of Saturn's moon Titan (44). The role of CO_2 in the haze formation process complicates understanding the atmospheric chemistry on the early Earth. Image of Earth appears courtesy of NASA/JPL/Space Science Institute.

early Earth (26, 27). Previous work by our group examined CH_4/CO_2 hazes using an electric discharge source (28), but a UV energy source is needed to interpret the results for the early Earth's atmosphere. Here, we use the results from $CH_4/CO_2/N_2$ photolysis to determine how similar the atmospheric chemistry on the early Earth may have been to Titan's current organic production and to explore the possibility of an early Earth haze layer (Fig. 1).

Results

An aerosol mass spectrometer (AMS) was the primary instrument used for particle analysis, providing aerosol mass spectra and quantification of aerosol mass. To probe the size and shape of the aerosols, experiments were performed by alternately using the AMS and a scanning mobility particle sizer (SMPS). A transmission electron microscope (TEM) was used to image a small sample of collected particles for corroboration of sizing data from the AMS and SMPS. The techniques used are described in *Materials and Methods*, and experimental conditions are further discussed in *Supporting Text*, which is published as supporting information on the PNAS web site.

Titan Simulations. Mixtures of 10, 1.6, 1, 0.1, 0.05, 0.01, 0.005, 0.002, and 0.001% CH_4 in N_2 were photolyzed with the UV lamp, and aerosol products were analyzed with the AMS. Contrary to previous results with an electric discharge (10), the chemical composition of the photochemical aerosols did not change appreciably with CH_4 concentration. In the electric discharge, the gas molecules, including N_2, are dissociated completely, and product formation includes ion chemistry. With the UV lamp, however, the photolysis leads to the formation of radicals, which go on to generate particles. Also, the UV light is not energetic enough to dissociate N_2. The difference in the chemistry initiated with each energy source is a likely explanation for the differences observed using the two excitation sources.

A representative particle mass spectrum obtained from UV photolysis of a 0.1% CH_4/N_2 mixture is shown in Fig. 2. The pattern observed in this spectrum is typical of long, stable hydrocarbon chains. Major peaks are separated by intervals of 14, 13, and 12 amu, indicative of chains formed by (-CH_2-), (-CH-), and (-C-) groups, respectively. Peaks that stand out from the pattern, such as 77 and 91 amu, are consistent with fragment ions for benzene and toluene, respectively. These species may serve as the building blocks for larger aromatic molecules. Even at the low concentrations observed here, the presence of aromatics is of interest because these molecules are extremely stable, can absorb in the UV and visible, and are ubiquitous throughout the universe. Additionally, benzene is the largest hydrocarbon species identified in Titan's atmosphere thus far (2, 29).

A C/H ratio was estimated from the aerosol spectrum by assuming that the mass fragment peaks were comprised only of carbon and hydrogen atoms. This is a logical assumption, because the UV lamp is not energetic enough to dissociate the

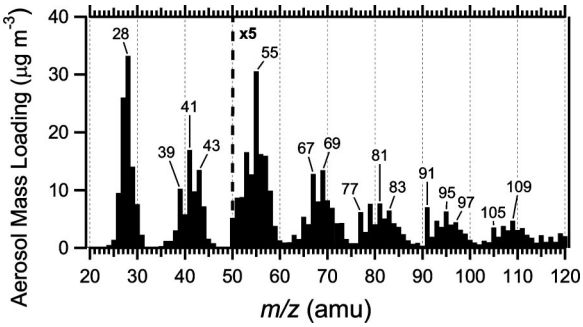

Fig. 2. Averaged mass spectrum for aerosols formed in 0.1% CH_4 in N_2. This spectrum is a representative spectrum for all aerosols produced in a range of mixtures of CH_4 in N_2. Data to the right of the dashed line at 50 amu are multiplied by 5 for ease of viewing. Prominent peaks are discussed in the text.

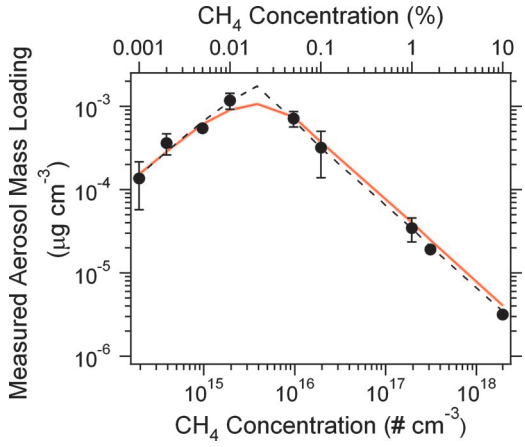

Fig. 3. Aerosol mass production trends for CH_4/N_2 experiments as a function of CH_4 concentration and mixing ratio. The data presented with black circles are derived from integrating the mass spectrum at each CH_4 concentration. The red solid line shows the amount of particle mass calculated from the photochemistry model developed from mechanism A. The black dashed line shows the amount of particle mass calculated from the model developed from mechanism B.

N_2 background gas. For example, a fragment peak at m/z 53 amu is assumed to represent a fragment with the formula C_4H_5, therefore containing four carbon atoms and five hydrogen atoms. The intensity ($\mu g \cdot m^{-3}$) of the fragment peak is then used to calculate a total number of C and H atoms present at that m/z ratio. This is repeated and summed for each fragment peak in the spectrum from 25 to 300 amu. The C/H ratio was determined in this way to be ≈0.6 for the 0.1% CH_4 spectrum (Fig. 2), which is consistent with unsaturated hydrocarbons. A table of compositional ratios from other studies of collected haze aerosols is given in Sarker *et al.* (11), and the average C/H ratio was found to be ≈0.75. It should be noted, however, that the experiments listed in the table were performed with an electrical discharge source, and thus also included N atoms. The analysis presented in this work agrees best with Sagan *et al.* (30), who report a C/H of 0.62 for particles generated with a spark discharge applied to a 10% CH_4/N_2 mixture.

Although the aerosol mass spectral signature was independent of the CH_4 mixing ratio, the amount of aerosol varied with CH_4 concentration. The aerosol production at different CH_4 concentrations was calculated by integrating the aerosol mass spectra and is shown in Fig. 3. It can be seen that the aerosol production initially increases with added CH_4, peaks near 0.02% CH_4, and then decreases with further increases in CH_4. This behavior can be qualitatively understood in terms of the optical depth of CH_4 in our cell with respect to the Lyman-α wavelength (121.6 nm), where most of the CH_4 dissociation is expected to occur. When the concentration is <0.02%, the reaction chemistry is CH_4-limited, and there is an increase in aerosol product with increasing CH_4. At CH_4 concentrations >0.02% CH_4, the reaction cell is optically thick at Lyman-α and all these photons are absorbed by the CH_4 molecules present. In this photon-limited regime, we expect a plateau in aerosol formation, yet there is a decrease in aerosol production with increased CH_4 concentration. The observed decrease in aerosol production is likely due to a decrease in the conversion of an intermediary species into aerosol products.

Two mechanisms are proposed here to understand the aerosol production trend from photochemistry of CH_4/N_2 atmospheres within the reaction cell. The primary assumption is that the photochemistry of CH_4 leads to the production of an intermediate, A, which in turn generates aerosol product. Mechanism A describes particle formation as a result of photolysis of the intermediate. In this mechanism, increased CH_4 shields the hydrocarbon intermediate and therefore decreases the aerosol formation rate at high CH_4 abundances.

Mechanism A

$$CH_4 + h\upsilon \rightarrow A \quad [1]$$

$$A + h\upsilon \rightarrow \text{aerosol products.} \quad [2]$$

Mechanism B describes particle formation from the reaction of intermediate molecules. In this mechanism, the intermediate can also react with CH_4, producing simple saturated gaseous hydrocarbons, thus reducing the formation of aerosol products.

Mechanism B

$$CH_4 + h\upsilon \rightarrow A \quad [1]$$

$$A + A \rightarrow \text{aerosol products} \quad [3]$$

$$A + CH_4 \rightarrow \text{nonaerosol products.} \quad [4]$$

These mechanisms have been used to develop equations to fit the data, and the fits are shown alongside the AMS data in Fig. 3. The models and their derivation are given in *Supporting Text*.

Either mechanism may be used to explain the trend observed in the AMS data, and we are unable to determine which one provides a more accurate model for the reaction chamber. However, both mechanisms demonstrate the same basic processes: (*i*) aerosol generation depends on initial CH_4 photolysis, and (*ii*) the formation and reaction of intermediate species is an integral step in aerosol production.

In addition to aerosol mass, we have examined the physical properties of the particles to determine how well they represent the features of Titan hazes. Aerosol size distributions were measured with the AMS and SMPS to provide particle diameter and information on morphology. The AMS measures particle size in terms of a vacuum aerodynamic diameter (D_{va}), which is related to particle shape and density, and the SMPS measures a mobility diameter (D_m), which is related to aerosol shape. The representative size distributions from both instruments are shown for 0.1% CH_4 in Fig. 4*a*. The average D_{va} observed is 36.5 ± 3.4 nm, and the average D_m is 46.3 ± 3.5 nm. Other workers have shown that an effective particle density, ρ_{eff}, for spherical particles can be found by relating these two diameters:

$$\rho_{eff} = \rho_0 \frac{D_{va}}{D_m} = \rho_m \cdot S, \quad [5]$$

where ρ_0 is the unit density (1 $g \cdot cm^{-3}$), ρ_m is the material density of the particle, and S is the Jayne shape factor (28, 31–33). Eq. **5** shows that the ρ_{eff} is proportional to the material density but also depends on S, which is equal to one for spherical particles, but is less than one for nonspherical aerosols (34). Using this analysis, the ρ_{eff} of the particles was determined to be ≈0.79 ± 0.09 $g \cdot cm^{-3}$. This density is similar to the material density of 0.8 $g \cdot cm^{-3}$, which is typical for materials composed of large hydrocarbon molecules, suggesting the particles are spherical (31). For spherical particles, the geometric diameter is equal to D_m (31), and therefore the laboratory aerosols should be ≈50 nm in diameter.

The aerosols produced from the 0.1% CH_4/N_2 gas mixture were also collected for imaging in the TEM, as shown in Fig. 4*b*. The TEM image shows geometric size and shape, and thus provides a complementary analysis to the *in situ* size distributions. Fig. 4*b* shows the particles to be approximately round in shape, an indication of sphericity. The average particle diameter

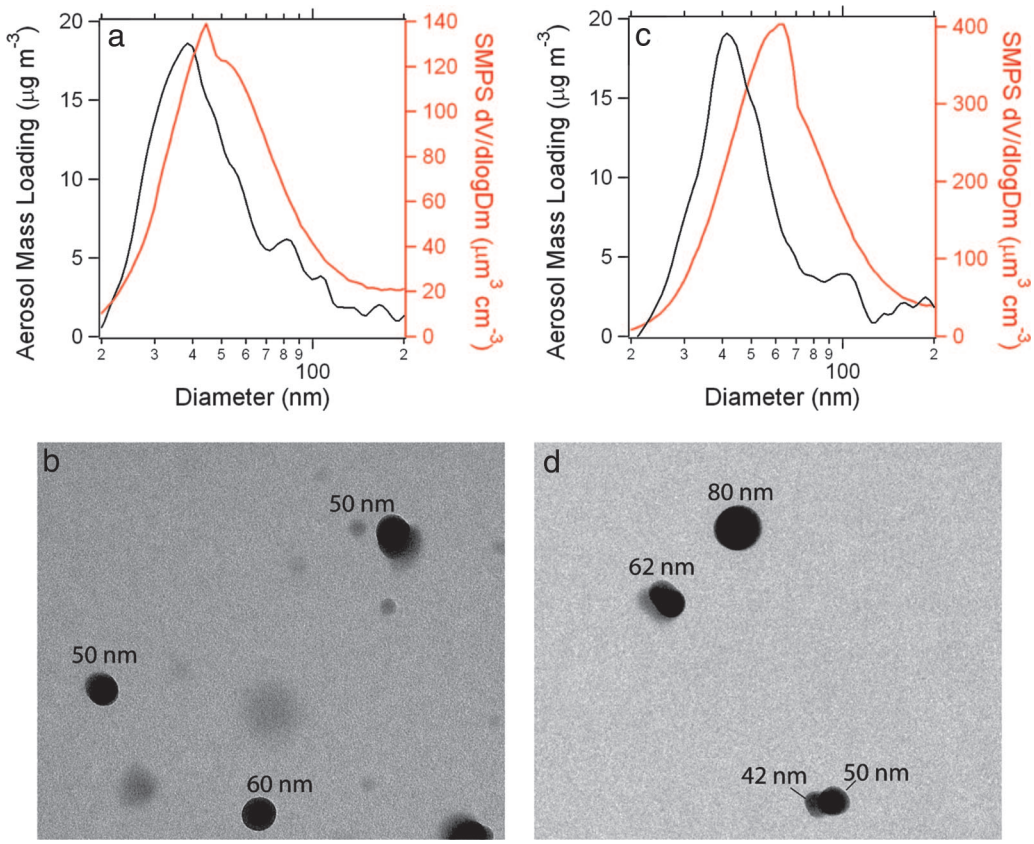

Fig. 4. Physical dimensions for aerosol analogs for Titan and early Earth. The black lines represent the particle traces from the AMS, measured for the m/z 41 fragment, as a function of D_{va}. The red lines represent the volume distribution measured by the SMPS, as a function of D_m. (*a*) Size distributions for aerosols produced in 0.1% CH_4 in N_2. The average D_{va} is 36.5 ± 3.4 nm, and the average D_m is 46.3 ± 3.5 nm. (*b*) TEM image of particles collected from the 0.1% CH_4 mixture described in *a*. Magnification was set at ×92,000, and particle sizes are indicated. The average particle diameter observed with the TEM was ≈50 nm. (c) Size distributions for aerosols produced in 0.1% CH_4/0.1% CO_2 in N_2 (C/O = 1). The average D_{va} is 34.4 ± 5.5 nm, and the average D_m is 54.5 ± 7.2 nm. (*d*) TEM image of particles collected from the C/O = 1 mixture described in *c*. Magnification was set at ×64,000, and particle sizes are indicated. The average particle diameter observed with the TEM was ≈50 nm.

observed in the TEM was ≈50 nm, in agreement with the D_m measurement.

We believe that we are observing the monomer aerosols because the particles measured have small diameters and appear to be spherical in shape. In combination with the absorptive properties of the aerosols, the size and shape are important elements in understanding how they will behave optically in the atmosphere. Models of Titan aerosols have determined that the aerosols are likely fractal aggregates of small spherical monomers, with the monomers having radii of ≈30–90 nm (35). *In situ* measurements taken from the Huygens Probe show that the monomers appear to be ≈50 nm in radius (36), or 100 nm in diameter, which is within a factor of two of the size observed here. The small particle sizes and spherical shapes observed in the laboratory indicate that the particles formed are spherical monomers and not fractal aggregates.

Early Earth Simulations. To investigate photochemical haze production on the early Earth, aerosol formation was studied in mixtures of CH_4 and CO_2. These experiments focused on a simulated atmosphere in which the CH_4 mixing ratio was held at 0.1%, and the CO_2 mixing ratio was varied from 0 to 0.5%. These mixing ratios are considered to be reasonable for the early Earth after the origin of life (23). The series of mass spectra obtained for particles generated in the early Earth simulation is shown in Fig. 5. Fig. 5*a* shows the spectrum for aerosols produced with the least amount of CO_2, which closely resembles the hydrocarbon signature observed when no CO_2 is present in the gas mixture. Some peaks that are indicative of alkane and alkene fragments are highlighted in the spectrum at m/z values of 39, 41, 43, and 55. The pattern observed at $m/z > 50$ amu is characteristic of the presence of hydrocarbon chains in the aerosol molecules. As the C/O ratio is decreased, the intensity of these large mass peaks diminishes. This loss indicates that the products of photochemistry at low C/O ratios are either molecules with lower molecular weights or with less stable chains. The aromatic peaks at 77 and 91 amu also decrease with increasing CO_2 in the starting gas mixture, indicating that there are fewer aromatic structures in these haze aerosols.

A peak that is continuously prominent across all experiments is that at m/z 28 amu. The time-of-flight traces for m/z 28 show this mass peak is a fragment of a larger molecule present in aerosol form, likely the $C_2H_4^+$ hydrocarbon fragment. For the experiments including CO_2, the m/z 28 peak may also contain contributions from a CO^+ fragment, as observed in other studies involving AMS analysis of oxygenated organics (37).

In the spectrum for particles produced with the highest CO_2 mixing ratio, shown in Fig. 5*e*, the hydrocarbon chains provide a small contribution to the particle signal, and new m/z peaks appear prominent. The main peaks identified in this spectrum are at 30 and 44 amu, which are consistent with the oxygenated organic fragments CH_2O^+ and COO^+, respectively. Particle signals confirm that these fragments are not gas-phase peaks. The oxygenated fragments may arise from larger molecules

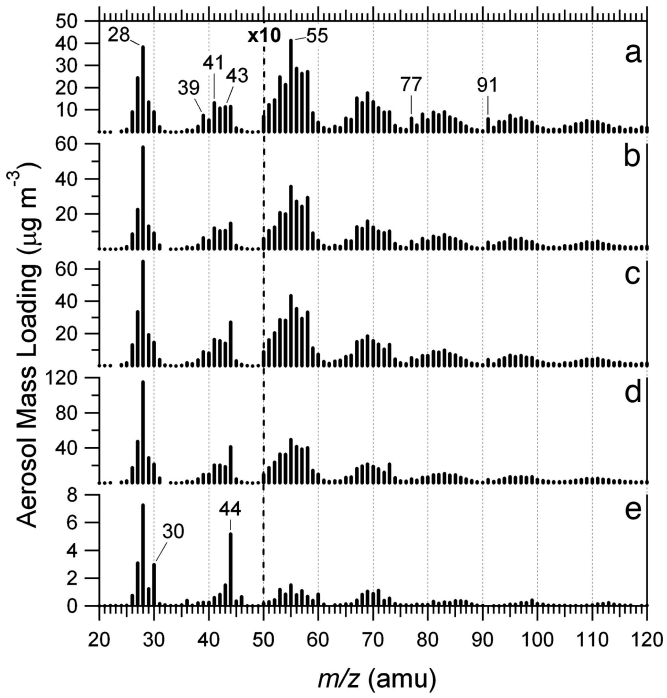

Fig. 5. Averaged mass spectra for standard early Earth simulations. Gas mixtures are composed of 0.1% CH_4 and 0.02% CO_2, C/O = 3 (*a*), 0.05% CO_2, C/O = 1.5 (*b*), 0.1% CO_2, C/O = 1 (*c*), 0.11% CO_2, C/O = 0.95 (*d*), and 0.5% CO_2, C/O = 0.6 (*e*). Data to the right of the dashed line at 50 amu are multiplied by 10 for ease of viewing. The spectrum for 0.1% CH_4 with no CO_2 added was shown in Fig. 2.

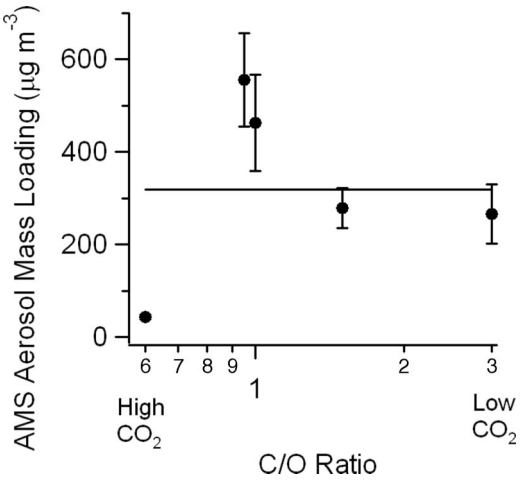

Fig. 6. Total aerosol mass produced as a function of the C/O ratio of the starting gas mixture. For all points CH_4 is at 0.1%. The filled circles are data derived from integrating the AMS mass spectra. The horizontal line shows the mass production from the CH_4-only experiments. Error bars are represented by the standard deviation of all experiments performed. The data at a C/O ratio of 1 show an average enhancement factor of $\beta = 1.5$ for aerosol production in the experiments with C/O = 1 as compared with the CH_4-only experiments.

containing COO and CO groups, such as carboxylic acids and aldehydes, or chains with oxygen substitutions, such as ethers. The photodissociation of CO_2 leads to the release of O radicals that may then be incorporated into hydrocarbon reactions, thus generating the oxygenated functional groups. The amount of oxygen incorporation in aerosols can be estimated for the lowest C/O ratio, if it is assumed that the peaks at m/z 30 and 44 are comprised entirely of the oxygenated fragments CH_2O^+ and COO^+. This estimation gives an oxygen content of 12% by mass. This value may be a lower limit on the oxygen incorporation, because it only considers two fragment peaks. However, if the mass peaks contain contributions from other fragments, then we may be overestimating the amount of oxygen.

The variation of chemical composition with C/O ratio seen in Fig. 5 shows that there is a marked increase in the abundance of aliphatic and aromatic species as the C/O ratio increases. The increase in stable hydrocarbon chains is also indicated by the increase in $m/z > 65$ amu peaks. Additionally, as the hydrocarbons increase in relative abundance, the oxidized organic signatures decrease. There appears to be an obvious transition in the chemical nature of the particles near a CH_4/CO_2 ratio of unity (Fig. 7, which is published as supporting information on the PNAS web site).

All experiments and analysis were repeated for gas mixtures of 1% CH_4 in N_2 with varying CO_2, at the same C/O ratios. Although not presented here, the results are qualitatively equivalent to those shown for the lower CH_4 concentration. This finding suggests that the chemical composition of the photochemical haze aerosols depends more on the C/O ratio than on the absolute concentrations of CH_4 and CO_2.

In addition to observing changes in the particle composition, the AMS is also used to determine the aerosol mass production as a function of C/O ratio, shown in Fig. 6. Although the mass changes only slightly when the C/O ratio >1, there was an increase in particle production observed when the CH_4 and CO_2 concentrations were approximately equal. This is an unexpected result, because aerosols were not predicted to form below a C/O ratio of 1 (38), and previous experiments with an electric discharge reported a decrease in aerosol production with added CO_2 (28). According to chemical schemes presented in the literature, as CH_4 and CO_2 are photolyzed, they are dissociated into the molecular and radical species H_2, CO, CH_2, CH, H, and O (12, 39). For aerosol production, only reactive pathways that lead to condensed phase products are of interest. Condensable products can only be formed if some hydrogen is removed from the system, either by forming H_2 or other gas-phase products. Otherwise, the dissociation products may recombine to CH_4 or other saturated low-molecular-weight hydrocarbons, such as C_2H_6. These hydrocarbons remain in the gas phase and thus do not contribute to aerosol formation. When O atoms are released from CO_2 photolysis, these can react with the H, thereby preventing it from recombination to form CH_4. In this way, the presence of a certain amount of CO_2 may favor particle growth, as displayed in Fig. 6. At a C/O ratio of 1, the release of one oxygen atom from CO_2 photolysis is at the correct stoichiometric ratio to combine with two H atoms from CH_4 photolysis and form H_2O. This would encourage the polymerization of -CH_2- groups and consequently lead to a maximum in aerosol formation. However, when the C/O ratio is dropped, there is more O available to terminate the hydrocarbon molecules and inhibit long-chain growth. Thus, having too much CO_2 will ultimately terminate aerosol formation, as seen at a C/O of 0.6.

Aerosol production at C/O ratios near 1 may also be enhanced because of the inclusion of oxygen in the aerosol chemical composition. Organic molecules with terminal oxygen groups, such as aldehydes and carboxylic acids, have lower vapor pressures than chains that contain the same number of carbons but no oxygen. Thus, as the chemical composition of the haze aerosols shifts to contain oxygenated functional groups, the lower vapor pressure of the reaction products may lead to a higher rate of condensation into aerosol mass. This vapor pressure effect may help explain the peak in aerosol production observed at a C/O ratio of 1, where there appears to be a signal for oxidized organics. At very low C/O ratios, however, the

oxidation appears to inhibit the formation of condensable aerosol material.

Simulated early Earth aerosols were also examined for particle size and morphology, using the methods described earlier. The representative size distributions from both sizing instruments are shown for a C/O ratio of 1 in Fig. 4*c*, and appear close in diameter, indicating that the particles may be somewhat spherical in shape (31). Particle size did not appear to vary much with starting gas mixture. For C/O ratios from 3 to 0.95, the average D_{va} is 34.4 ± 5.5 nm, and the average D_m is 54.5 ± 7.2 nm. An estimated value for ρ_{eff} was determined to be ≈0.64 ± 0.13 g·cm^{-3}. A TEM image for aerosols collected from the 0.1% CH_4/0.1% CO_2 experiment is shown in Fig. 4*d*. In this image, it can be seen that the particles are approximately round in shape and have an average diameter ≈50 nm.

This ρ_{eff} is low compared with the material density values for various oxygenated organic species similar to the structures suggested by the mass spectra. These densities range from 0.8 g·cm^{-3} for acids and aldehydes to 1.5 g·cm^{-3} for aromatic and polycarboxylic acids (40). The low ρ_{eff} could indicate either that the aerosols have irregular shapes or that they are spherical with internal voids (31). However, the TEM image suggests that the particles may be nearly spherical, despite the low ρ_{eff} calculated from the measurements. Thus, the aerosols might contain internal voids that lower the ρ_{eff}, although these are not visible in the image. The geometric particle diameter observed in the TEM image is similar to the D_m, and this is also an indication that the particles are approximately spherical.

Implications for Early Earth

The particle size results presented above may have implications for the climate of early Earth. The early climate is often compared with that on present-day Titan. The sunlight on Titan is much dimmer than on the current Earth, partly because of its distance from the Sun but also because of the haze layer. The light is diffuse, due to scattering by the haze, and the color of the sky is orange (36). As on Titan, the light available to the early Earth's surface would be strongly influenced by attenuation of the haze layer. This is related to the optical properties of the haze material, but also the size and shape of the aerosols. Pavlov *et al.* (22) found in their model that particle size was critical in determining the UV shielding of a haze layer. Using the approximate particle radius of 0.025 μm from this study, the model would predict a haze layer that is optically thick in the UV region but relatively thin in the visible, therefore making it climatically feasible to have a UV shield. Pavlov *et al.* also showed that for particles >0.2 μm in diameter, a significant UV shield would correspond with significant loss of visible sunlight, which is undesirable because it would cool the Earth's surface. Previous experiments forming early Earth aerosols using a discharge source readily formed fractal aggregates with diameters >0.10 μm (28), which would be expected to show different optical properties compared with the spherical monomers (41). These fractal aggregates are consistent with microphysical models for Titan (42). Thus, the UV shielding of a photochemically produced haze layer on early Earth would depend strongly on whether the particles observed eventually form fractal aggregates in the atmosphere.

The climatic effect would also depend on the particle mass produced. The results from the $CH_4/CO_2/N_2$ experiments can be used to infer a possible haze production rate on the early Earth. At the high altitudes where atmospheric CH_4 photolysis is expected, the CH_4 partial pressure would be low enough that the environment is CH_4-limited with respect to Lyman-α photons. Thus, the aerosol production trends shown in Fig. 3 for the CH_4-limited case ([CH_4] < 0.02%) should be similar to that on Titan or the early Earth. Two chemical reaction mechanisms have been used to fit the data in Fig. 3, and both show that aerosol mass production is directly proportional to CH_4 concentration in the CH_4-limited region (see *Supporting Text*). In the equation derived from Mechanism A,

$$C \propto I_0^2 n_c, \quad [6]$$

where C is the aerosol concentration (μg·cm^{-3}), I_0 is the light intensity at Lyman-α (photons·s^{-1}), and n_c is the CH_4 concentration (molecules·cm^{-3}). In the equation derived from Mechanism B,

$$C \propto I_0 n_c \quad [7]$$

in the CH_4-limited regime.

Using the relationships derived from experimental results, the observed production rate of aerosols on Titan can be used to suggest a possible haze formation rate on the early Earth. A simple proportionality is used to estimate possible photochemical haze formation on the early Earth based on the correlations discussed above:

$$F_{EE} = \beta \cdot F_T \cdot \left(\frac{I_{0EE}}{I_{0T}}\right)^m \cdot \left(\frac{\chi_{cEE}}{\chi_{cT}}\right), \quad [8]$$

where F_{EE} and F_T are the aerosol fluxes (g·cm^{-2}·s^{-1}) on early Earth (*EE*) and Titan (*T*); m is an exponent equal to either 2 (Mechanism A) or 1 (Mechanism B); I_0 is the solar flux on early Earth and Titan; and χ_c is the atmospheric mixing ratio of CH_4 on early Earth and Titan. The values of F_T, I_0, and χ_c for each planet, along with results of the calculation, F_{EE}, are given in Table 1. The experimental data displayed in Fig. 6 show that when the CH_4 and CO_2 are approximately equal, there is ≈1.5 times as much aerosol formation as in a CH_4-only atmosphere. To account for this, an average enhancement factor of $\beta = 1.5$ has been used in the equation to estimate aerosol formation for the early Earth.

The above calculation yields a range of possible aerosol production rates from 4 × 10^{-13} to 8 × 10^{-11} g·cm^{-2}·s^{-1}, if the atmospheric CH_4 concentration is ≈1,000 ppmv. This is a plausible scenario for the postbiotic Earth (23), when methanogenic bacteria were likely present (21). Most of the uncertainty comes from the different dependence on I_0 in Mechanisms A and B. This range of production rates correlates to a terrestrial global aerosol production of 1 × 10^{13} to 3 × 10^{15} g·year^{-1}. This calculated aerosol production rate is in reasonable agreement with Pavlov *et al.*'s (22) photochemical model estimate of ≈4 × 10^{13} g of C per year. This rate is also comparable with the carbon burial rate in the Archean, which is estimated to have been approximately the same as the current carbon burial rate of 5 × 10^{13} g of C per year (43). Thus, the analysis in this work suggests

Table 1. Haze production on Titan and the early Earth

	Titan	Early Earth (postbiotic estimation)
I_0, Solar flux at Lyman-α, photons·cm^{-2}·s^{-1}	6.2 × 10^9*	1.4 × 10^{12}†
X_c	0.016‡	0.001§
F, Aerosol production flux, g·cm^{-2}·s^{-1}	1.2 × 10^{-14}¶	8 × 10^{-11} (Mechanism A) 4 × 10^{-13} (Mechanism B)
Aerosol production, g·year^{-1}	8 × 10^{10}¶	3 × 10^{15} (Mechanism A) 1 × 10^{13} (Mechanism B)

*Current solar flux at 9.5 AU.
†Current solar flux at 1 AU × 2.5 to account for stronger EUV emissions in the Archean (20, 52).
‡From Flasar *et al.* (3).
§From Pavlov *et al.* (23).
¶From Toon *et al.* (53).

that, on the postbiotic Earth, haze formation may substantially impact the temperature and habitability of the planet (22, 24, 44), the cycling of organic material within the biosphere (28), and the geologic record (45, 46).

The value for the CH_4 concentration on the prebiotic Earth is not certain, because the magnitude of abiotic CH_4 production from possible sources such as mid-Atlantic ridges (47) is unknown. However, it is possible that the abiotic sources may have supported a mixing ratio of CH_4 up to 1×10^{-4} (48). With this amount of CH_4 in the atmosphere, the CO_2 mixing ratio on an unfrozen early Earth is expected to be at least 3×10^{-4} (23). The results presented in Fig. 6 show that, at a CH_4/CO_2 ratio of 0.33 (a C/O ratio of 0.67), there would still be haze production. As discussed in Tian *et al.* (20), previous estimates for the delivery of organic material to the prebiotic Earth rely on synthesis in hydrothermal vents or exogenous delivery from interstellar dust particles. These sources have been estimated to be on the order of 2×10^{11} g of C per year. Using Eq. **8**, organic production was estimated for a CH_4 mixing ratio on the prebiotic Earth of $\approx 1 \times 10^{-4}$ and a C/O ratio of at least 0.6. Fig. 6 shows that a C/O ratio of 0.6 has a β factor of 0.1, as compared with CH_4-only production. This yields an organic production of 10^{11} to 10^{13} g·year^{-1}, which is comparable with or greater than other estimated sources. Although the C/O ratio may have been <0.6 in the prebiotic environment, it has been suggested that there could still be organic haze due to increased H_2 (20). Thus, atmospheric haze chemistry could have the potential to deliver more organic material to the early Earth than has been estimated for hydrothermal vents or exogenous delivery. Atmospheric CH_4/CO_2 photolysis could therefore have proved a very efficient process for the delivery of large amounts of organics to the Earth's surface both before and after the emergence of life. This production may have allowed life to flourish globally, and not just in localized environments as currently favored in some theories for the origin of life.

Materials and Methods

Photochemical hazes were studied in a flow system to avoid wall effects or secondary reactions that can arise in a static system, as discussed by Thompson *et al.* (49). Gas mixture production, aerosol generation, and particle analysis techniques have been described in detail (10, 28). Experiments were performed with concentrations of CH_4 and CO_2 in N_2 from 0.001 to 10%. The reaction cell was held at 600 Torr and room temperature. The critical new element of the particle generation system is the use of a UV light source to drive photochemistry of CH_4 and CO_2 within the chamber. A water-cooled deuterium lamp with MgF_2 windows (Hamamatsu, Bridgewater, NJ, L1835) was inserted directly into the reaction cell. The lamp is a continuum light source emitting from 115 to 400 nm, with maximum output between 115 and 165 nm. The primary wavelength for CH_4 photolysis is expected at the Lyman-α line at 121.6 nm, with a cutoff around 145 nm. The deuterium lamp has a peak near 121 nm, and the emission spectrum overlaps well with the CH_4 absorption spectrum. Thus, it is an appropriate source to initiate CH_4 photolysis. Details on the UV lamp characterization are given in *Supporting Text*.

Several analytical methods were used in this study to probe the chemical and physical properties of the organic aerosols. The AMS, developed and built by Aerodyne Research (Billerica, MA; ref. 34), obtains quantitative data without exposing aerosols to laboratory air, providing averaged mass spectra of the bulk nonrefractory aerosol. Instrument design, modes of operation, and data analysis techniques are described by Allan *et al.* (50), Jimenez *et al.* (51), and Jayne *et al.* (34). Use of this instrument in previous studies of this nature can be found in Trainer *et al.* (10, 28). In this study, the vaporization temperature was 600°C, and the electron energy was 70 eV.

The SMPS measures the size distribution of aerosol populations and was used in conjunction with the AMS to gather information regarding the size distribution of the haze aerosols produced in our experiments. Use of the SMPS has been described (28).

The TEM was used to image collected haze aerosols to observe their size and morphology. The aerosols were collected by placing carbon-coated TEM grids on top of a filter that was installed in-line with the aerosol flow. The particles were collected for ≈ 8 h and then imaged on a Phillips CM10 (FEI, Hillsboro, OR) scope.

We thank J. F. Kasting and M. A. Smith for valuable comments on this manuscript. This material is based on work supported by National Aeronautics and Space Administration (NASA) Grants NNG04GM42G, NNG05GA53G, and EXB03–0015-0010 issued through the Office of Space Science. Partial support was also received from the NASA Astrobiology Institute through the University of Colorado Center for Astrobiology and the National Science Foundation. M.G.T. and H.L.D. were supported by fellowships through the NASA Graduate Student Research Program and NASA Office of Space Science. M.A.T. gratefully acknowledges support from the John Simon Guggenheim Memorial Foundation.

1. Porco CC, Baker E, Barbara J, Beurle K, Brahic A, Burns JA, Charnoz S, Cooper N, Dawson DD, Del Genio AD, *et al.* (2005) *Nature* 434:159–168.
2. Waite JH, Niemann H, Yelle RV, Kasprzak WT, Cravens TE, Luhmann JG, McNutt RL, Ip WH, Gell D, De La Haye V, *et al.* (2005) *Science* 308:982–986.
3. Flasar FM, Achterberg RK, Conrath BJ, Gierasch PJ, Kunde VG, Nixon CA, Bjoraker GL, Jennings DE, Romani PN, Simon-Miller AA, *et al.* (2005) *Science* 308:975–978.
4. Shemansky DE, Stewart AIF, West RA, Esposito LW, Hallett JT, Liu XM (2005) *Science* 308:978–982.
5. Israel G, Szopa C, Raulin F, Cabane M, Niemann HB, Atreya SK, Bauer SJ, Brun J-F, Chassefiere E, Coll P, *et al.* (2005) *Nature* 438:796–799.
6. Coll P, Coscia D, Smith N, Gazeau MC, Ramirez SI, Cernogora G, Israel G, Raulin F (1999) *Planet Space Sci* 47:1331–1340.
7. Khare BN, Sagan C, Arakawa ET, Suits F, Callcott TA, Williams MW (1984) *Icarus* 60:127–137.
8. Imanaka H, Khare BN, Elsila JE, Bakes ELO, McKay CP, Cruikshank DP, Sugita S, Matsui T, Zare RN (2004) *Icarus* 168:344–366.
9. Khare BN, Bakes ELO, Imanaka H, McKay CP, Cruikshank DP, Arakawa ET (2002) *Icarus* 160:172–182.
10. Trainer MG, Pavlov AA, Jimenez JL, McKay CP, Worsnop DR, Toon OB, Tolbert MA (2004) *Geophys Res Lett* 31:L17S08.
11. Sarker N, Somogyi A, Lunine JI, Smith MA (2003) *Astrobiology* 3:719–726.
12. Yung YL, Allen M, Pinto JP (1984) *Astrophys J Suppl Ser* 55:465–506.
13. Wilson EH, Atreya SK (2003) *Planet Space Sci* 51:1017–1033.
14. Adamkovics M, Boering KA (2003) *J Geophys Res* 108:5092–5105.
15. Tran BN, Ferris JP, Chera JJ (2003) *Icarus* 162:114–124.
16. Tran BN, Joseph JC, Ferris JP, Persans PD, Chera JJ (2003) *Icarus* 165:379–390.
17. Coustenis A (1995) *Earth Moon Planets* 67:95–100.
18. Clarke DW, Ferris JP (1997) *Orig Life Evol Biol* 27:225–248.
19. Rye R, Kuo PH, Holland HD (1995) *Nature* 378:603–605.
20. Tian F, Toon OB, Pavlov AA, De Sterck H (2005) *Science* 308:1014–1017.
21. Woese CR (1987) *Microbiol Rev* 51:221–271.
22. Pavlov AA, Brown LL, Kasting JF (2001) *J Geophys Res* 106:23267–23287.
23. Pavlov AA, Kasting JF, Brown LL, Rages KA, Freedman R (2000) *J Geophys Res* 105:11981–11990.
24. McKay CP, Lorenz RD, Lunine JI (1999) *Icarus* 137:56–61.
25. Coll P, Bernard JM, Navarro-Gonzalez R, Raulin F (2003) *Astrophys J* 598:700–703.
26. Miller SL (1953) *Science* 117:528–529.
27. Stribling R, Miller SL (1987) *Orig Life Evol Biol* 17:261–273.
28. Trainer MG, Pavlov AA, Curtis DB, McKay CP, Worsnop DR, Delia AE, Toohey DW, Toon OB, Tolbert MA (2004) *Astrobiology* 4:409–419.
29. Niemann HB, Atreya SK, Bauer SJ, Carignan GR, Demick JE, Frost RL, Gautier D, Haberman JA, Harpold DN, Hunten DM, *et al.* (2005) *Nature* 438:779–784.
30. Sagan C, Khare BN, Lewis JS (1984) in *Saturn*, eds Gehrels T, Matthews MS (Univ of Arizona Press, Tucson), pp 788–807.
31. DeCarlo P, Slowik JG, Worsnop DR, Davidovits P, Jimenez JL (2004) *Aerosol Sci Technol* 38:1185–1205.

32. Jimenez JL, Bahreini R, Cocker DR, Zhuang H, Varutbangkul V, Flagan RC, Seinfeld JH, O'Dowd C, Hoffmann T (2003) *J Geophys Res Atmos* 108:4318–4342.
33. Jimenez JL, Bahreini R, Cocker DR, Zhuang H, Varutbangkul V, Flagan RC, Seinfeld JH, O'Dowd C, Hoffmann T (2003) *J Geophys Res* 108:4733.
34. Jayne JT, Leard DC, Zhang X, Davidovits P, Smith KA, Kolb CE, Worsnop DR (2000) *Aerosol Sci Technol* 33:49–70.
35. Rannou P, Cabane M, Chassefiere E, Botet R, McKay CP, Courtin R (1995) *Icarus* 118:355–372.
36. Tomasko MG, Archinal B, Becker T, Bezard B, Bushroe M, Combes M, Cook D, Coustenis A, de Bergh C, Dafoe LE, *et al.* (2005) *Nature* 438:765–778.
37. Zhang Q, Alfarra MR, Worsnop DR, Allan JD, Coe H, Canagaratna MR, Jimenez JL (2005) *Environ Sci Technol* 39:4938–4952.
38. Zahnle KJ (1986) *J Geophys Res* 91:2819–2834.
39. Toublanc D, Parisot JP, Brillet J, Gautier D, Raulin F, McKay CP (1995) *Icarus* 113:2–26.
40. Pang Y, Turpin BJ, Gundel LA (2006) *Aerosol Sci Technol* 40:128–133.
41. West RA (1991) *Appl Opt* 30:5316–5324.
42. McKay CP, Coustenis A, Samuelson RE, Lemmon MT, Lorenz RD, Cabane M, Rannou P, Drossart P (2001) *Planet Space Sci* 49:79–99.
43. Lasaga AC, Berner RA, Garrels RM (1985) in *The Carbon Cycle and Atmospheric CO_2: Natural Variations Archean to Present*, eds Sundquist E, Broecker W (Am Geophys Union, Washington, DC), pp 397–411.
44. Sagan C, Chyba C (1997) *Science* 276:1217–1221.
45. Pavlov AA, Kasting JF, Eigenbrode JL, Freeman KH (2001) *Geology* 29:1003–1006.
46. Holland HD (2002) *Geochim Cosmochim Acta* 66:3811–3826.
47. Kelley DS, Karson JA, Fruh-Green GL, Yoerger DR, Shank TM, Butterfield DA, Hayes JM, Schrenk MO, Olson EJ, Proskurowski G, *et al.* (2005) *Science* 307:1428–1434.
48. Kasting JF, Brown LL (1998) in *The Molecular Origins of Life*, ed Brack A (Cambridge Univ Press, New York), pp 35–56.
49. Thompson WR, Henry TJ, Schwartz JM, Khare BN, Sagan C (1991) *Icarus* 90:57–73.
50. Allan JD, Jimenez JL, Williams PI, Alfarra MR, Bower KN, Jayne JT, Coe H, Worsnop DR (2003) *J Geophys Res Atmos* 108:4090–4099.
51. Jimenez JL, Jayne JT, Shi Q, Kolb CE, Worsnop DR, Yourshaw I, Seinfeld JH, Flagan RC, Zhang X, Smith KA, *et al.* (2003) *J Geophys Res Atmos* 108:8425–8437.
52. Dorren JD, Guinan EF (1994) *Astrophys J* 428:805–818.
53. Toon OB, McKay CP, Griffith CA, Turco RP (1992) *Icarus* 95:24–53.